Active Control for Flutter Suppression: An Experimental Investigation

E. Papatheou[1], N.D. Tantaroudas[1], A. Da Ronch[2],

J.E. Cooper[3] and J.E. Mottershead[1]

[1] Centre for Engineering Dynamics, University of Liverpool, Liverpool L69 3GH, UK
[2]Engineering and the Environment, University of Southampton, Southampton, SO17 1BJ, UK
[3] Dept. of Aerospace Engineering, University of Bristol, Bristol, BS8 1TR, UK

Abstract

This paper describes an experimental study involving the implementation of the method of receptances to control binary flutter in a wind-tunnel aerofoil rig. The aerofoil and its suspension were designed as part of the project. The advantage of the receptance method over conventional state-space approaches is that it is based entirely on frequency response function measurements, so that there is no need to know or to evaluate the system matrices describing structural mass, aeroelastic and structural damping and aeroelastic and structural stiffness. There is no need for model reduction or the estimation of unmeasured states, for example by the use of an observer. It is demonstrated experimentally that a significant increase in the flutter margin can be achieved by separating the frequencies of the heave and pitch modes. Preliminary results from a complementary numerical programme using a reduced-order model, based on linear unsteady aerodynamics, are also presented.

1. Introduction.

Aeroservoelasticity (ASE) is the engineering science of structural deformation interacting with aerodynamic and control forces [1-2]. It is an essential component for the design of next-generation flexible and maneuverable aircraft and sensorcraft, manned or unmanned, as well as for new flight control systems (FCS). One of the goals of ASE is to overcome the dynamic instability phenomenon of *flutter*, which can lead to catastrophic structural failure when the aircraft structure starts to absorb energy from the surrounding aerodynamic flow [3-5]. The suppression of flutter, achieved by either passive or active means [6-8], may be considered as an inverse eigenvalue problem [9], often referred to as eigenvalue assignment. Passive techniques for flutter suppression may require mass balancing and structural stiffness or shape modifications. Although such passive techniques are considered very robust in their performance, they introduce additional weight and possibly constraints that may be prohibitive to aircraft performance. Alternatively, by supplying active control forces using sensors and

actuators embedded in the aircraft structure, the desired performance may be achieved actively. For example, forces originating from the coupling of the structure with the aerodynamic flow may be modified and flutter suppressed by actively controlling the ailerons or reshaping the surface of wings (morphing) to optimize a performance objective.

For an adequately designed aircraft, flutter will occur outside the desired flight envelope, at some matched dynamic pressure and Mach number. Both military and commercial aircraft designs require a 15% flutter free margin beyond the designed speed and altitude envelope [3]. In order to develop the next-generation aircraft or spacecraft, or to improve the performance of existing aircraft, the extension of flutter-free margins needs to be realized by active suppression techniques using existing control surfaces. However, it should be noted that no aircraft is currently flown beyond its flutter speed through the incorporation of a flutter suppression system.

The main objective of this study is to demonstrate in principle that by using on-board sensor and control surfaces, the flutter boundaries of a given flight envelope can be extended using active control techniques based upon vibration measurements. In recent years, the theory and application of pole placement by the receptance method have been developed in a series of papers [10]-[14] based upon this idea. The main idea of the receptance method is to obtain and utilize transfer function data from available sensors and actuators, and to design control gains purely based upon such measurements. The receptance approach has a number of significant advantages over conventional pole-placement methods, either cast in the first-order state-space or as second-order matrix polynomials [15]. There is no need to know or to evaluate the structural matrices that usually contain various modelling assumptions and errors, and must be brought into agreement with test data by model updating.

A further approximation for aeroelastic systems is that the unsteady aerodynamic forces must also be modelled, typically using a frequency domain analysis. For ASE applications, it is usual to approximate the frequency domain aerodynamics, extracted from the aeroelastic influence coefficient (AIC) matrix at a set of discrete frequencies [3,16] into the time domain, via a rational fraction approximation of the aerodynamics. This procedure, generally dependent upon finite element codes such as MSC-NASTRAN, ZAERO or ASTROS, is rendered completely unnecessary by the receptance method which captures the coupled aeroelastic behaviour in the measurement. The word *receptance* comes from the first theoretical papers which assumed force inputs and displacement outputs, but is now a misnomer, since the inputs and outputs may be any measurable quantities. This means that the measured inputs and outputs may, for example, be input and output voltage signals to the actuators and from the sensors, so that the sensor and actuator dynamics are included in the measured data. The sensors and actuators do not have to be collocated. There is no requirement to estimate unmeasured state variables by an observer or Kalman filter, and no need for model reduction. This may be understood by consideration of the system equations, in receptance form they are displacement equations, whereas by conventional methods force equations are formed using dynamic stiffnesses. It is seen that a complete displacement equation is formed for each measured degree of freedom, provided each of the external forces applied by a small number of actuators is measured. Conversely the force equations are not complete unless all the degrees of

freedom are measured; this requires estimation of the unmeasured state variables.

For ASE control application, the available matrix of receptances is usually quite modest in size, determined entirely by the number of available on-board sensors and actuators. For example, in order to compute the receptance transfer function, the input might be the voltage applied to a motor for movement of a control surface, and the output may be obtained from embedded accelerometers. The number of sensors is generally equal to the number of eigenvalues to be assigned, provided that the eigenvalues are observable. In principle a single actuator can assign all the eigenvalues, which must be simple and controllable, and may be implemented using time-varying control requiring the in-flight measurement of receptances and determination of control gains.

This report describes the theory of the method of receptances and its implementation on a wind-tunnel aerofoil rig, which was designed and constructed as part of this project. The receptance method is implemented by fitting rational fraction polynomials to measured frequency response functions (FRFs), in the present case the inputs are the voltages applied to a power amplifier supplying a 'V' stack piezo-actuator and the outputs are laser sensor displacement signals (and velocities obtained by numerical differentiation in dSPACE[1]). The measured FRFs include not only the dynamics of the system but also of the actuator and sensors and the effects of A/D and D/A conversion, numerical differentiation and the application of high-pass and low-pass Butterworth filters in dSPACE. Successful pole placement is achieved in preliminary tests and finally flutter-margin extension is demonstrated by separating the frequencies of the heave and pitch modes.

[1] http://www.dspace.com/en/inc/home.cfm

2. Preliminary Theory

The governing equation of an aeroelastic system can be written as [3]

$$\boldsymbol{A}\ddot{\boldsymbol{q}} + (\rho v\boldsymbol{B} + \boldsymbol{D})\dot{\boldsymbol{q}} + (\rho v^2\boldsymbol{C} + \boldsymbol{E})\boldsymbol{q} = \boldsymbol{p} \qquad (1)$$

where, $\boldsymbol{A}, \boldsymbol{B}, \boldsymbol{C}, \boldsymbol{D}, \boldsymbol{E}$ are the structural inertia, aerodynamic damping, aerodynamic stiffness, structural damping and structural stiffness matrices respectively, $\boldsymbol{q}(t)$ is the vector of generalised coordinates, $\boldsymbol{p}(t)$ is the vector of control forces. The aerodynamic forces, for a chosen Mach number and reduced frequency, are expressed as additional contributions to the system matrices. In equation (1) these terms appear as matrices $\boldsymbol{B}$ and $\boldsymbol{C}$ which, in general, are frequency dependent. Often these forces are combined together in the form of the aeroelastic influence coefficient (AIC) matrix at a set of discrete frequencies. Here, a simplified aeroelastic modeling approach will be used that still maintains the key characteristics of unsteady aerodynamic behaviour [3].

For the open-loop homogenous system, using separation of variables,
$\boldsymbol{q}(t) = \sum_{j=1}^{2n} \alpha_j \boldsymbol{\varphi}_j \exp(\lambda_j t)$,
and the eigenvalue equation of the j^{th} mode is expressed as

$$\left(\lambda_j^2\boldsymbol{A} + (\rho v\boldsymbol{B} + \boldsymbol{D})\lambda_j + (\rho v^2\boldsymbol{C} + \boldsymbol{E})\right)\boldsymbol{\varphi}_j = \boldsymbol{0} \qquad (2)$$

Where α_j is the j^{th} modal coordinate. The complex eigenvalues in equation (2) may be written in terms of the j^{th} damping and natural frequency, which are determined from the real and imaginary parts of the characteristic eigenvalues (or poles). For the models used in this report, the matrices, $\boldsymbol{A}, \boldsymbol{B}, \boldsymbol{C}, \boldsymbol{D}, \boldsymbol{E}$, are strictly real and constant, with the

eigenvalues (and eigenvectors) appearing in complex conjugate pairs such that

$$\lambda_{j,n+j} = -\zeta_j \omega_j \pm \mathrm{i}\omega_j \sqrt{\left(1-\zeta_j^2\right)}$$
$$j = 1, 2, \ldots, n \qquad (3)$$

For more accurate models, the aerodynamic matrices $\boldsymbol{B}$ and $\boldsymbol{C}$ are complex and depend upon the reduced frequency. This approximation does not affect the accuracy of the control approach, which is the main focus of this work.

The real part of the eigenvalues defines the stability of the system and, when the real part of the eigenvalues λ_j in equation (3) is positive, the system is unstable and results in flutter. The system considered here has linear structural and aerodynamic models, so non-linear phenomena such as Limit Cycle Oscillations (LCOs) cannot occur. For all other values of the real part of the eigenvalues, the aeroelastic system is either stable or marginally stable.

Flutter of the aircraft, or its components, is a dynamic instability associated with the aeroelastic system which involves interaction and coupling of modes (wing bending/torsion, wing torsion/control surface, wing/engine, etc.) that results in energy being extracted from the airstream leading to negatively damped modes and unstable oscillations. For a given Mach number, at some critical speed (flutter speed) the eigenvalues exhibit instability, leading to sustained oscillations which can result in catastrophic failure. In a flutter analysis the eigenvalues, and hence the natural frequencies and damping ratios, are computed for varying speeds, altitudes and Mach numbers, and the critical flutter speeds determined. In aeroelastic control, the goal is to suppress flutter, or extend the flutter boundaries, by assigning stable poles using feedback control forces, usually supplied by available control surfaces e.g. ailerons.

The system matrices in equations (1) and (2) depend upon the aeroelastic system, the number of degrees of freedom, and on the position and size of the control surfaces. The objective of the approach is to use the Receptance Control Method in order to define the control forces required to place the closed loop poles in such a manner that the onset of flutter is delayed. This is achieved by placing the closed loop poles at different, more advantageous, positions in the complex plane compared to those of the open loop system.

3. Active Control by the Method of Receptances

The approach used in this work will be demonstrated using a binary aeroelastic system, shown in Figure 1, which incorporates a control surface as part of a closed loop feedback system. Note that the control surface is not a flexible degree of freedom, but provides a means to impart a force onto the aerofoil which is proportional to the control angle β.

The receptance matrix of the open loop system may be expressed in the complex Laplace domain as the inverse of the aeroelastic dynamic stiffness matrix,

$$\boldsymbol{H}(s) = \left(\boldsymbol{A}s^2 + (\rho v \boldsymbol{B} + \boldsymbol{D})s + (\rho v^2 \boldsymbol{C} + \boldsymbol{E})\right)^{-1} \quad (4)$$

However, in practice it is determined from frequency response functions (FRFs) estimated from power and cross spectral densities of force and response measurements using well known procedures, for example described by Bendat and Piersol [17]. Curve fitting of the estimated $\boldsymbol{H}(\mathrm{i}\omega)$, for example by the PolyMAX routine [18], allows the determination of $\boldsymbol{H}(s)$ by substituting s for $\mathrm{i}\omega$ in the curve-fitted approximation; this approach was demonstrated in active vibration control by Tehrani *et al.* [19]. In this paper it is assumed that the matrix of

receptances can be determined from in-flight measurements of aeroelastic inputs and outputs. It can be demonstrated [19] that any input and output signals may be used in aeroelastic eigenvalue assignment, in which case the dynamics of actuators and sensors (including the effects of time delay) may be included in the measurement, rendering unnecessary the need for mathematical models to approximate the behavior of actuators and sensors.

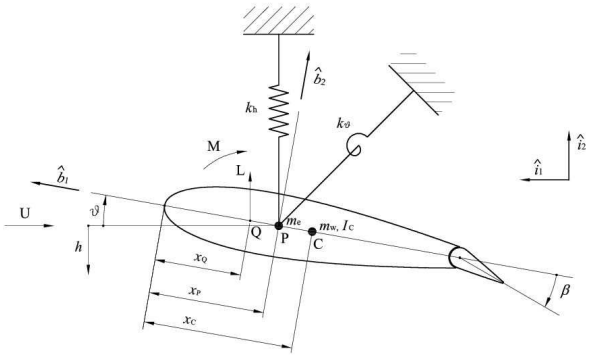

Figure 1: Binary Airfoil Configuration with Control Surface.

The method depends upon a very useful result from the linear algebra, namely the Sherman-Morrison formula, which produces a modified inverse matrix, $\overline{\boldsymbol{Z}}^{-1} = (\boldsymbol{Z} + \boldsymbol{uv}^T)^{-1}$, when a known rank 1 modification, $\boldsymbol{uv}^T$, and original inverse matrix, $\boldsymbol{Z^{-1}}$, are available such that

$$\overline{\boldsymbol{Z}}^{-1}(s) = \boldsymbol{Z^{-1}}(s) - \frac{\boldsymbol{Z}^{-1}(s)\boldsymbol{u}(s)\boldsymbol{v}^T(s)\boldsymbol{Z}^{-1}(s)}{1+\boldsymbol{v}^T(s)\boldsymbol{Z}^{-1}(s)\boldsymbol{u}(s)} \quad (5)$$

In single-input control, the control force is typically given by

$$\boldsymbol{p}(t) = \boldsymbol{b}u(t) \quad (6)$$

where

$$u(t) = \boldsymbol{f}^t\dot{\boldsymbol{q}} + \boldsymbol{g}^T\boldsymbol{q} \quad (7)$$

for displacement and velocity feedback, where the gains $\boldsymbol{f}$ and $\boldsymbol{g}$ are such that the closed loop system has new (closed-loop) complex poles $\mu_{j,n+j}$, $j = 1, \dots, n$.

By combining equations (1), (6) and (7), we get

$$\boldsymbol{A}\ddot{\boldsymbol{q}} + (\rho v\boldsymbol{B} + \boldsymbol{D} + \boldsymbol{bf}^T)\dot{\boldsymbol{q}} + (\rho v^2\boldsymbol{C} + \boldsymbol{E} + \boldsymbol{bg}^T)\boldsymbol{q} = \boldsymbol{0} \quad (8)$$

or in the complex Laplace domain

$$(\boldsymbol{A}s^2 + (\rho v\boldsymbol{B} + \boldsymbol{D} + \boldsymbol{bf}^T)s + (\rho v^2\boldsymbol{C} + \boldsymbol{E} + \boldsymbol{bg}^T))\boldsymbol{q}(\boldsymbol{s}) = \boldsymbol{0} \quad (9)$$

and so the closed-loop eigenvalue equation becomes

$$(\boldsymbol{A}\mu_j^2 + (\rho v\boldsymbol{B} + \boldsymbol{D} + \boldsymbol{bf}^T)\mu_j + (\rho v^2\boldsymbol{C} + \boldsymbol{E} + \boldsymbol{bg}^T))\boldsymbol{\psi}_j = \boldsymbol{0} \quad (10)$$

Where μ_j, $\boldsymbol{\psi}_j$, μ_{n+j}, $\boldsymbol{\psi}_{n+j}$, $j = 1, \dots, n$ denote the closed-loop eigenvalues and eigenvectors in complex-conjugate pairs.

Evidently, from equation (9), the open-loop system is changed by the rank 1 modification, $\boldsymbol{b}(s\boldsymbol{f} + \boldsymbol{g})^T$. Therefore, the closed-loop receptance matrix is given from the Sherman-Morrison formula as

$$\overline{\boldsymbol{H}}(s) = \boldsymbol{H}(s) - \frac{\boldsymbol{H}(s)\boldsymbol{b}(s\boldsymbol{f}+\boldsymbol{g})^T\boldsymbol{H}(s)}{1+(s\boldsymbol{f}+\boldsymbol{g})^T\boldsymbol{H}(s)\boldsymbol{b}} \quad (11)$$

and, from the denominator of equation (11), the control gains f, g must be chosen so that the equations

$$\left.\begin{aligned} 1 + \left(\mu_j\boldsymbol{f} + \boldsymbol{g}\right)^T\boldsymbol{H}(\mu_j)\boldsymbol{b} = \boldsymbol{0} \\ 1 + \left(\mu_{n+j}\boldsymbol{f} + \boldsymbol{g}\right)^T\boldsymbol{H}(\mu_{n+j})\boldsymbol{b} = \boldsymbol{0} \end{aligned}\right\} \quad j = 1, \dots, n \quad (12)$$

are satisfied for the assignment of the closed-loop eigenvalues in complex-conjugate pairs $\mu_{n+j} = \mu_j^\star$.

Re-arranging and combining equations (12) into a single matrix expression leads to

$$\boldsymbol{G}\begin{pmatrix}\boldsymbol{g}\\ \boldsymbol{f}\end{pmatrix} = \begin{pmatrix}-1\\ \vdots\\ -1\end{pmatrix} \tag{13}$$

with

$$\boldsymbol{G} = \begin{bmatrix} \boldsymbol{r}_1^T & \mu_1\boldsymbol{r}_1^T \\ \boldsymbol{r}_2^T & \mu_2\boldsymbol{r}_2^T \\ \vdots & \vdots \\ \boldsymbol{r}_{2n}^T & \mu_{2n}\boldsymbol{r}_{2n}^T \end{bmatrix} \tag{14}$$

where

$$\left.\begin{aligned} \boldsymbol{r}_j(\mu_j) &= \boldsymbol{H}(\mu_j)\boldsymbol{b} \\ \boldsymbol{r}_{n+j}(\mu_{n+j}) &= \boldsymbol{H}(\mu_{n+j})\boldsymbol{b} \end{aligned}\right\} \tag{15}$$

which allows the determination of f and g by inversion of the matrix G. Ram and Mottershead [10] showed that

I. $\boldsymbol{G}$ is invertible when the system is controllable and the poles μ_j , $j = 1,2,\dots 2n$ are distinct, and
II. $\boldsymbol{f}$ and $\boldsymbol{g}$ are real when $\boldsymbol{G}$ is invertible and the set μ_j , $j = 1,2,\dots 2n$ are closed under conjugation [9].

When $\boldsymbol{G}$ is a square matrix there is a unique solution for $(\boldsymbol{g} \quad \boldsymbol{f})^T$ and when the system (14) is under-determined (fewer poles to be assigned than the number of gain terms, $\boldsymbol{f}$, $\boldsymbol{g}$) then a minimum norm solution is available for the minimization of control effort. Alternatively, in the latter case, the gains may be chosen that assign the chosen eigenvalues while at the same time minimizing the sensitivity of the assigned poles to inaccuracy and noise in the measured receptances. A robust pole-placement approach to noise on the measured receptances is described by Tehrani et al. [14].

4. The Experimental Rig

The wind tunnel experiment consists of a working section containing a NACA0018 aerofoil (chord = 0.35 m, span = 1.2m), supported by adjustable vertical and torsional leaf springs. The aerofoil can be modelled as a 2D system with pitch and heave degrees of freedom as illustrated in Figure 1.

The design allows the adjustment of the stiffnesses of the vertical and torsional springs, k_h and k_ϑ. The maximum air speed for the wind tunnel used is around 20 m/s. The aim of the design is to explore regions close to the flutter speed of the system.

The vertical spring arrangement is shown in Figure 2. By varying the clamp location in the direction shown in the figure, it is possible to vary the stiffness of the vertical springs, one on each side of the wind tunnel, which support the wing (attached to the shaft on the left of the figure). The vertical stiffness is variable in the range 200 to 23000 N/m.

The adjustable torsional spring is shown in Figure 3. By moving the device in the direction indicated by the arrows it is possible to increase or reduce the torsional stiffness in the range 10 to 320 Nm/rad.

Using these ranges of stiffness, it is possible to vary the flutter speed of the aeroelastic system approximately between 10 and 70 m/s. The open working section (with sides removed and separated from the wind tunnel) is shown in Figure 4. A torsion bar is used in order to maintain the same vertical displacement on the two sides of the test section. The external mass of the system was calculated to be around 6.5 Kg.

Active vibration control described in [20, 21] is achieved by means of a 'V'-stack piezoelectric actuator shown in Figure 5 acting on the control surface of the wing, allowing a flap deflection of about ±7°. The actuator consists of two piezo-stacks (Noliac SCMAP09-H80-A01) in a 'V' formation. The flap is actuated when one arm of the 'V' is made to extend while the other retracts by an equal amount – caused by applying equal voltages to the two

piezo stacks but with 180° phase difference. Khron Hite wideband power amplifiers, model 7500, were used. The 'V' stack actuator [21] is known to behave as a pure gain provided that its natural frequency is well above the frequencies of the assigned poles.

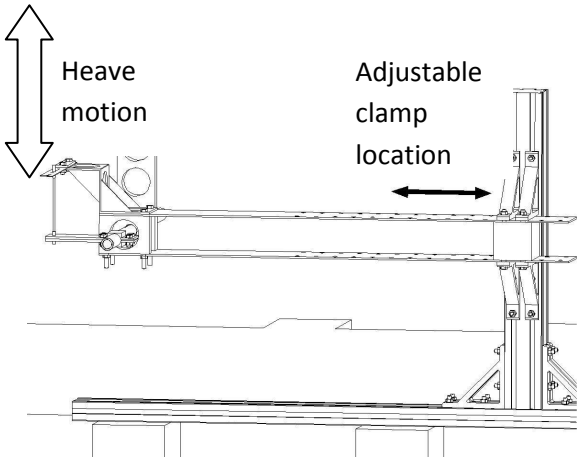

Figure 2: Adjustable Vertical Spring

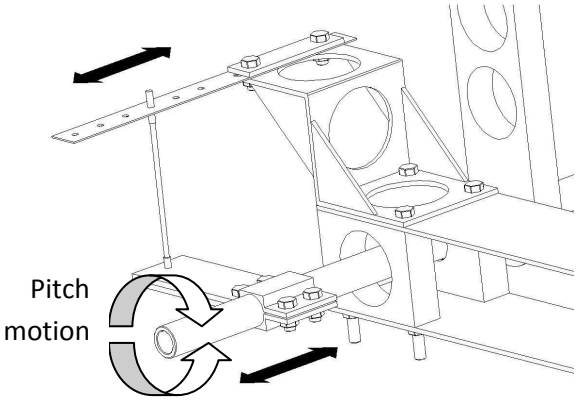

Figure 3: Adjustable Torsion Spring

The receptance method was applied with voltage input to the power amplifiers and displacement output, measured using two laser sensors KEYENCE LK-500 and LK-501. The laser sensors were mounted externally to the working section above a rigid horizontal bar attached to the aerofoil shaft. Separation of the sensors allowed the measurement of both vertical translation and rotation of the shaft (heave and pitch).

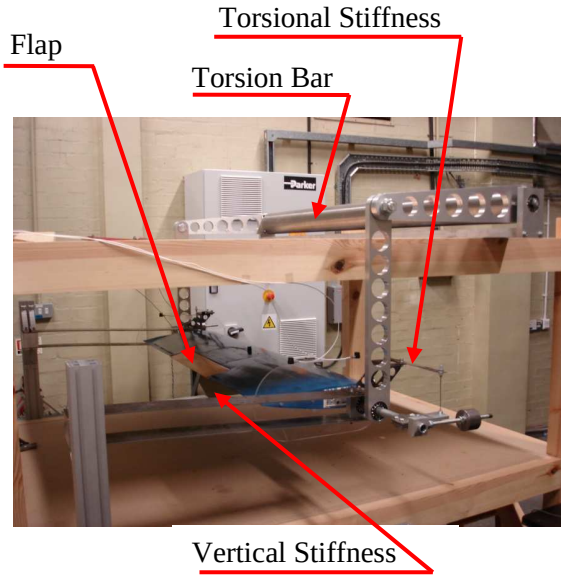

Figure 4: Open Working Section

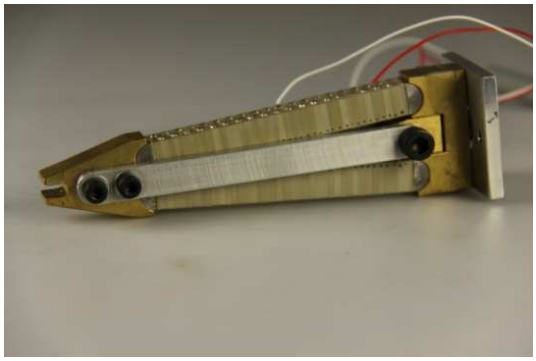

(a)

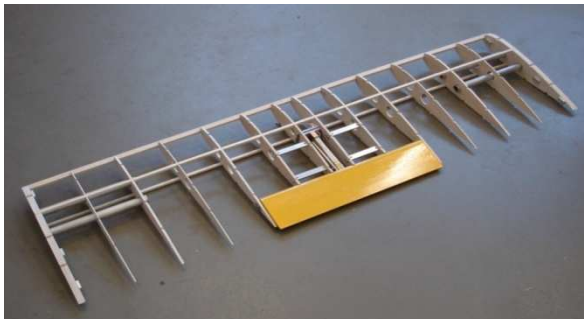

(b)

Figure 5 : (a) V-stack actuator; (b) Actuator In-Situ

5. Implementation of the Receptance Method

Frequency response functions (FRFs) relating the power amplifier input voltage v_β to the displacements x_1 and x_2 measured using the laser sensors were determined by stepped-sine testing using a SCADAS III LMS data acquisition system. The frequency range used was 5 to 30 Hz and the frequency resolution was 0.05 Hz.

Thus at a chosen wind speed v, the matrix $\boldsymbol{H}(\omega, v)$ in the theory of Section 4 above is given by the relationship,

$$\begin{bmatrix} h_{1,\beta} \\ h_{2,\beta} \end{bmatrix} v_\beta = \begin{pmatrix} x_1 \\ x_2 \end{pmatrix};$$

$$\boldsymbol{H}(\omega, v) = \begin{bmatrix} h_{1,\beta}(\omega, v) \\ h_{2,\beta}(\omega, v) \end{bmatrix} \tag{16}$$

where x_1 and x_2 are the measured displacements. The velocities $\dot{x}_1$ and $\dot{x}_2$ were calculated numerically using Simulink/dSPACE with a sampling rate of 10 kHz and a separate FRF $\dot{\boldsymbol{H}}(\omega, v)$ was determined as,

$$\begin{bmatrix} \dot{h}_{1,\beta} \\ \dot{h}_{2,\beta} \end{bmatrix} v_\beta = \begin{pmatrix} \dot{x}_1 \\ \dot{x}_2 \end{pmatrix};$$

$$\dot{\boldsymbol{H}}(\omega, v) = \begin{bmatrix} \dot{h}_{1,\beta}(\omega, v) \\ \dot{h}_{2,\beta}(\omega, v) \end{bmatrix} \tag{17}$$

The over-dot simply denotes that the FRF relates to the velocity and does not imply differentiation of $\boldsymbol{H}(\omega, v)$.

The open loop FRFs $\boldsymbol{H}(\omega, v)$ and $\dot{\boldsymbol{H}}(\omega, v)$ included not only the dynamics of the aerofoil system, but also of the power amplifier, the actuator, the sensors and the effects of A/D and D/A conversion, numerical differentiation of the measured displacements and high-pass and low-pass Butterworth filters with cut-off frequencies of of 1 Hz and 35 Hz respectively (also implemented in dSPACE).

Transfer functions $\boldsymbol{H}(s, v)$ and $\dot{\boldsymbol{H}}(s, v)$ may then be obtained by fitting rational fraction polynomials to the measured $\boldsymbol{H}(\omega, v)$ and $\dot{\boldsymbol{H}}(\omega, v)$. This was achieved using a pole-residue model (typically SDTools[2]).

Finally, the assignment of two pairs of complex-conjugate poles was achieved by the application of equation (13) with the matrix $\boldsymbol{G}$ given by,

$$\boldsymbol{G} = \begin{bmatrix} \boldsymbol{H}(\mu_1, v) & \dot{\boldsymbol{H}}(\mu_1, v) \\ \boldsymbol{H}(\mu_1^*, v) & \dot{\boldsymbol{H}}(\mu_1^*, v) \\ \vdots & \vdots \\ \boldsymbol{H}(\mu_2^*, v) & \dot{\boldsymbol{H}}(\mu_2^*, v) \end{bmatrix} \tag{18}$$

and $b = 1$ since there is a single actuator and may take an arbitrary value.

It should be noted that at no stage in this process is it necessary to know or to evaluate the matrices $\boldsymbol{A}, \boldsymbol{B}, \boldsymbol{C}, \boldsymbol{D}, \boldsymbol{E}$. Any assumption or mis-modelling of the structural- or aero-dynamics is not included and the performance of the resulting controller depends only upon the quality of the measured frequency response functions $\boldsymbol{H}(\omega, v)$ and $\dot{\boldsymbol{H}}(\omega, v)$.

6. Measurement of FRFs and Pole Placement

One objective of the design of the experimental rig was that the flexible modes of the aerofoil should be well separated from the sprung modes of the aerofoil system, in which the aerofoil is effectively rigid. It is these sprung modes, in pitch and heave, that are to be controlled. A preliminary modal test carried out with a small impact hammer revealed the first bending mode at 41 Hz and first torsion mode of the aerofoil at 47 Hz. There was a mode of the aerofoil support structure (the springs, linkages and torsion bar) at just over 20 Hz and it was important

[2] http://www.sdtools.com/

before implementing the controller to ensure that these modes will not be destabilized.

From equations (13) and (18), it is seen that the Nyquist stability criterion is satisfied when $\boldsymbol{H}^T(\omega, v)\boldsymbol{g} + \dot{\boldsymbol{H}}^T(\omega, v)\boldsymbol{f} = [h_{1,\beta} \quad h_{2,\beta}]\begin{pmatrix} g_1 \\ g_2 \end{pmatrix} + [\dot{h}_{1,\beta} \quad \dot{h}_{2,\beta}]\begin{pmatrix} f_1 \\ f_2 \end{pmatrix}$ does not encircle -1.

An example of curve-fitting to a measured FRF using SDTools is shown in Figure 6 for the case of a pitch mode at 3.9 Hz and a heave mode at 6.7 Hz and a wind speed of 7 m/s.

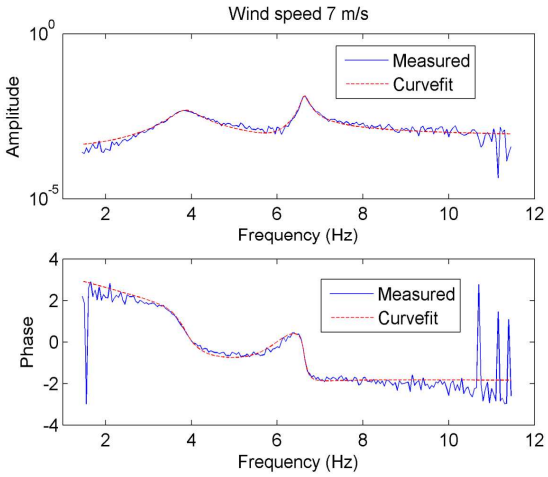

Figure 6. Measured and Curve-Fitted FRFs

An example of pole-placement is given in Figure 7, where (1) the frequency of the heave mode is shifted by a small amount from 6.83 Hz to 7 Hz and an increase of 0.5% damping is assigned and (2) the frequency of the pitch mode is shifted from 3.89 Hz to 3.5 Hz with an increase in damping of 1.5% assigned. The assigned poles are -0.8±44i and -2±22i and the gains are found to be $\boldsymbol{g} = (34.6 \quad 2.45)^T$, $\boldsymbol{f} = (0.734 \quad 0.427)^T$.

In another example, poles are assigned at -1.5±42.96i and -1.84±24.49i to achieve mainly an increase in damping of the heave mode. The corresponding gains are $\boldsymbol{g} = (-16 \quad -14)^T$ and $\boldsymbol{f} = (0.39 \quad 0.42)^T$. The time-domain response of the aerofoil in open- and closed-loop to an initial displacement is shown in Figure 8. It is seen that a significant reduction in vibration amplitude is achieved.

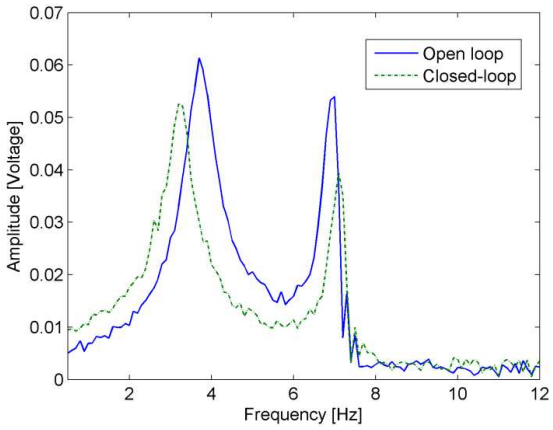

Figure 7. Measured Open- and Closed-Loop FRF after Application of Active Pole Placement

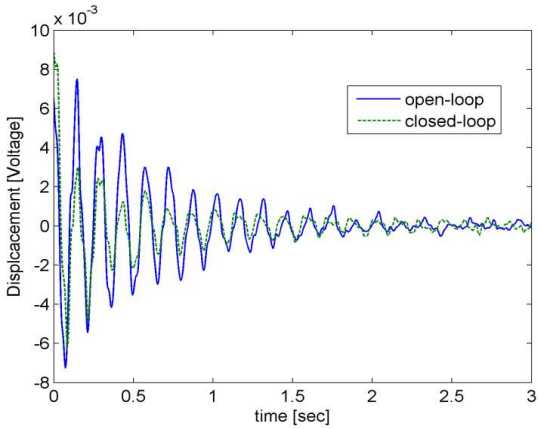

Figure 8. Displacement sensor time-domain response

7. Flutter Margin Control by Pole Placement

The experiments described in this section were carried out with the vertical and torsional srings adjusted to give a heave frequency of approximately 3.6 Hz and a pitch frequency of about 5.6 Hz. Tests were carried out to achieve an extended flutter margin by separating the heave and pitch frequencies.

The frequency spacing between the two modes is increased by pole assignment as seen in Figure 9. Pole assignment $\mu_{pitch} = -3.43 \pm 37.2\text{i}$, $\mu_{heave} = -1.24 \pm 24.7\text{i}$ is carried out at $v = 15\ \text{m/s}$ resulting in gains $\boldsymbol{g} = [-13.98 \quad 9.84]^{\text{T}}, \boldsymbol{f} = [-0.115 \quad 0.161]^{\text{T}}$. The same values of $\boldsymbol{g}$ and $\boldsymbol{f}$ were applied by the controller for air speeds from 6 to 15 m/s.

The Nyquist diagram, shown in Figure 10, is the plot of

$$[h_{1,\beta} \quad h_{2,\beta}]\begin{pmatrix} g_1 \\ g_2 \end{pmatrix} + [\dot{h}_{1,\beta} \quad \dot{h}_{2,\beta}]\begin{pmatrix} f_1 \\ f_2 \end{pmatrix}$$

as explained previously in Section 6. This plot was obtained for different gains than those given above, but gives a good indication of the stability of the system in the range $0.5 \leq \omega \leq 30$ Hz. It is seen that there is a gain margin of 5.2 and a phase margin of 36°, thereby indicating robust stability at $7\ \text{m/s}$.

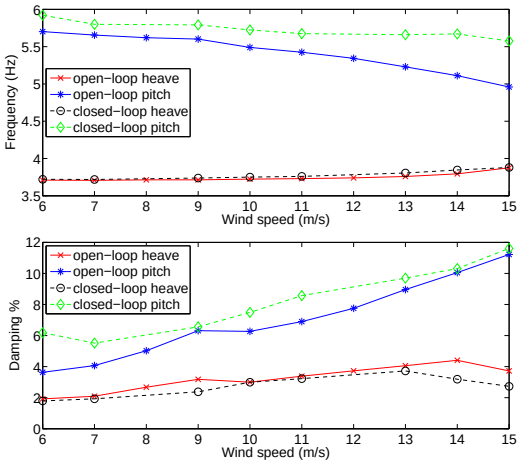

Figure 9. Frequency and Damping of Heave and Pitch Modes.

Figure 9b shows that separation of the modal frequencies is achieved mainly by increasing the frequency of the pitch mode, while the heave frequency remains mostly unchanged. The system was found to undergo quite large control-surface oscillations when an increase in pitch damping as well as in frequency was attempted. In Figures 9 and 11 typical eigenvalue trends leading eventually to flutter may be observed. It can be seen that the heave mode is not affected very much by control action whereas the poles of the pitch mode change considerably. In Figure 9 the frequency of the closed-loop pitch mode remains almost constant as v is increased, but there are signs that it begins to reduce after about 14 m/s. Also the damping of the closed-loop pitch mode is consistently higher than its open-loop counterpart. The system behaviour becomes very clear in Figure 11 where the locus of the closed-loop pitch mode is seen to move consistently further away from the imaginary axis increase in air speed and does not seem to be close to instability. At 15 m/s the poles of the pitch frequency are seen to be further away from the imaginary axis than those of the open loop system.

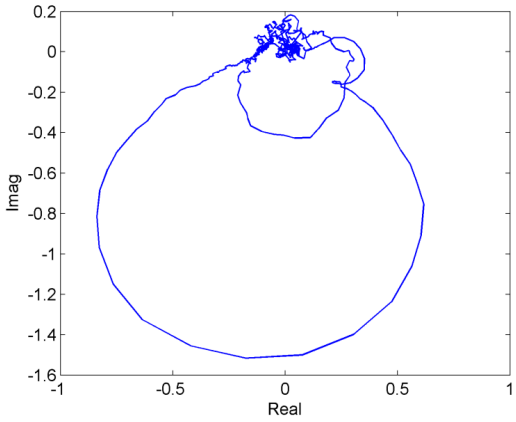

Figure 10. Nyquist Diagram: $v = 7\ \text{m/s}$.

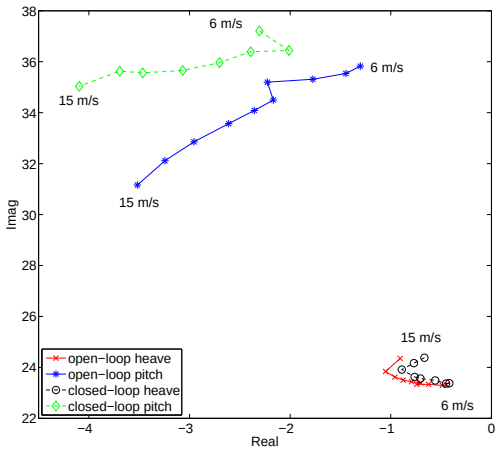

Figure 11. Root Locus with Air Speed.

The flutter margin for a two degree of freedom system (without structural damping) is given by the non-negative function [22-24] of either the open- or closed-loop eigenvalues that satisfies the Routh stability test,

$$F = \left[\left(\frac{\tilde{\omega}_2^2 - \tilde{\omega}_1^2}{2}\right) + \left(\frac{\sigma_2^2 - \sigma_1^2}{2}\right)\right]^2 + 4\sigma_1\sigma_2\left[\left(\frac{\tilde{\omega}_2^2+\tilde{\omega}_1^2}{2}\right) + 2\left(\frac{\sigma_2^2+\sigma_1^2}{2}\right)^2\right] - \left[\left(\frac{\sigma_2-\sigma_1}{\sigma_2+\sigma_1}\right)\left(\frac{\tilde{\omega}_2^2-\tilde{\omega}_1^2}{2}\right) + 2\left(\frac{\sigma_2+\sigma_1}{2}\right)^2\right]^2 \quad (19)$$

where $\sigma_j = -\zeta_j\omega_j;\ \tilde{\omega}_j = \omega_j\sqrt{(1-\zeta_j^2)};$ $j = 1,2.$

It can be shown that the flutter margin, F, is quadratic in the air speed v.

Figure 12 shows two curves obtained by fitting parabolas to experimental values of $F(v)$. The open-loop flutter margin is the full-line blue curve fitted through experimental points given by the red squares. The closed-loop flutter margin is represented by the dashed curve fitted through the experimental black circles. An increase in the flutter speed of 11.5% from 17.5 m/s to 19.5 m/s is predicted by using the method proposed by Dimitriadis and Cooper [24].

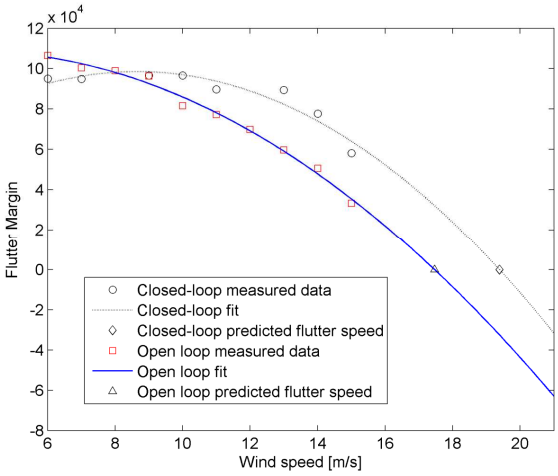

Figure 12. Flutter Margin by Separation of Heave and Pitch Frequencies.

8. Towards Integrating Simulation with Experiments

The experimental research described above was complemented by a parallel programme of numerical work in which the wind tunnel aerofoil rig was modelled using a three degree of freedom aerofoil section. A linear aerodynamic model based on strip theory and the incompressible two-dimensional classical theory of Theodorsen was used. The structural model was linear. More details on the modelling approach[3] and code validation against common test cases can be found in [25] and [26].

The aeroelastic parameters used for the simulations are μ = 69.0, $\overline{\omega}$ = 0.649, a_h = -0.33, x_α = 0.09, and r_α^2 = 0.40. Structural damping was included in the model to reproduce damping observed in the wind tunnel rig, ζ_{pitch} = 0.015, ζ_{heave} = 0.02. Symbols used here are standard parameters in the literature and their definitions can be found, for example, in [25].

The numerical model was first validated against wind tunnel measurements in predicting the damped frequency and damping ratio. A comparison is made in Fig. 13. The predictions are in good agreement with actual measurements. With increasing freestream speed, the damping of the coupled system increases. At the flutter point, which occurs for a speed of 17.63 m/s, the damping ratio becomes negative and a coalescence of the pitch and plunge modes is observed. The flutter point predicted by the numerical model compares well with the value of about 17.5 m/s extrapolated from measurements.

[3] The code can be obtained from A. Da Ronch, A.Da-Ronch@soton.ac.uk

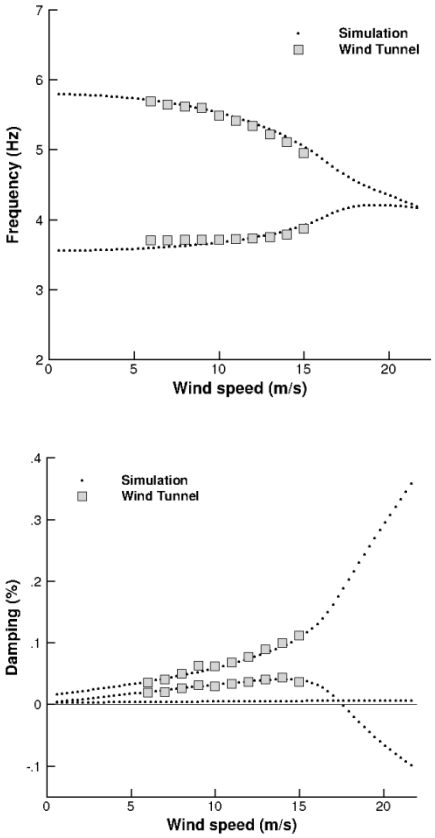

Figure 13. Damped frequency and damping ratio for varying freestream speed from simulation and wind tunnel measurements

The stability behaviour is traced throughout the speed range of interest solving for an eigenvalue problem of the coupled aeroelastic system. This information can then be used to design a controller to extend the flutter boundary. Preliminary work on this has been carried out and results will be presented in future work. There is, however, the question of the cost. The recursive solution of the eigenvalue problem is, in general, costly if the size of the system is large (see, for example, Ref. [27]). A promising alternative is based on the approach to model reduction reported in Ref. [25]. The generation of a reduced model is: a) straightforward for linear and nonlinear systems; b) independent of the underlying governing equations; and c) suitable for control applications. Here, the reduced model was parameterised with respect to the airspeed. This allows predicting the system response over a range of airspeeds using one single reduced model generated at a given speed. Figure 14 compares the free response to an initial perturbation in heave velocity obtained using the full model and the reduced order model at three different airspeeds. The full model was run at each airspeed and is taken to be the reference solution for the reduced model. The reduced model was generated once at the speed of 6.2 m/s. The predictions are in good agreement with the reference solution although the airspeed is increased by 50% from the point at which the reduced model is generated. Future work will focus on a) the use of the reduced model for a quick assessment of the stability behaviour of the aerofoil rig, and b) evaluating the impact of model fidelity on the flutter boundary extension of the wind tunnel rig.

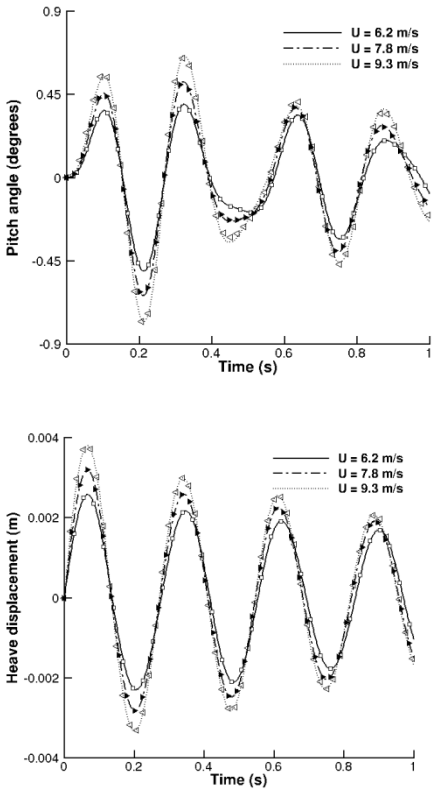

Figure 14. Free response in plunge and pitch: lines denote the full-order mode; symbols denote predictions of the reduced order model generated at 6.2 m/s

9. Conclusions

A wind-tunnel aerofoil test rig has been designed and built, making use of a single control surface operated by a 'V' stack piezo-actuator. Eigenvalues have been assigned successfully and control of flutter has been demonstrated using the receptance method and the flutter-margin prediction procedure. In the experiments carried out with this particular aerofoil system the flutter speed was increased by around 12 % when pole placement was applied to separate the heave and pitch frequencies. Pole placement to separate the heave and pitch frequencies was found to be effective in increasing the flutter speed. Preliminary results from a complementary numerical programme using a reduced-order model, based on linear unsteady aerodynamics, were presented.

Acknowledgement

The authors wish to acknowledge the support of EPSRC grant EP/J004987/01 and EOARD grant FA8655-10-1-3054.

References

1. H. Zimmerman, Aeroservoelasticity, *Computer Methods in Applied Mechanics and Engineering*, 90(13), 1991, 719-735
2. L. Librescu, Advances in Linear / Nonlinear Control of Aeroelastic Structural Systems, *Acta Mechanica*, 178, 2005, 147-186.
3. J.R. Wright & J.E. Cooper, Introduction to Aircraft Aeroelasticity and Loads, 2007, John Wiley.
4. Fung, Y., 1995, An *Introduction to the Theory of Aeroelasticity*, Dover (original 1955).
5. Hodges, D.H. and Pierce, G.A., 2002, *Introduction to Structural Dynamics and Aeroelasticity*, Cambridge University Press, 2002.
6. De Marqui, C. Jr., Belo, E. M., Marques, F. D., 2004, Wind-Tunnel Model and a Controller for Flutter Suppression, *45th AIAA/ASME/ASCE/AHS/ASC Structures, Structural Dynamics & Materials Conference*, 19-22 April 2004, Palm Springs, California, AIAA 2004-1854.
7. Njuguna, J., 2007, Flutter prediction, suppression and control in aircraft composite wings as a design prerequisite: A survey, *Structural Control and Health Monitoring*, 14, pp. 715–758.
8. Buttrill, Carey S., Bacon, Barton J., Heeg, Jennifer, and Houck, Jacob A., 1996, *Aeroservoelastic Simulation of an Active Flexible Wing Wind Tunnel Model*, NASA Technical Paper 3510.
9. Mottershead, J. E. and Ram, Y. M., Inverse eigenvalue problems in vibration absorption: passive modification and active control, *Mechanical Systems and Signal Processing,* 20(1), 2006, 5-44.
10. Ram, Y.M. and Mottershead, J.E., 2007, Receptance method in active vibration control, *American Institute of Aeronautics and Astronautics Journal*, 45(3), pp. 562-567.
11. Mottershead, J.E., Tehrani, M.G., James, S. and Ram, Y.M., 2008, Active vibration suppression by pole-zero placement using measured receptances, *Journal of Sound and Vibration,* 311(3-5), pp. 1391-1408.
12. Mottershead, J.E., Tehrani, M.G. and Ram, Y.M., 2009, Assignment of eigenvalue sensitivities from receptance measurements, *Mechanical Systems and Signal Processing*, 23(6), pp.1931-1939.
13. Ram, Y.M., Singh, A. and Mottershead, J.E., 2009, State feedback with time delay, *Mechanical Systems and Signal Processing*, 23(6), pp. 1940-1945.

14. Tehrani, M. G., Mottershead, J. E., Shenton, A. T., and Ram, Y. M., 2010, Robust pole placement in structures by the method of receptances, *Mechanical Systems and Signal Processing*, doi:10.1016/j.ymssp.2010.04.005.
15. Tisseur, F., and Meerbergen, K., The Quadratic Eigenvalue Problem, *SIAM Review*, Vol. 43, No. 2, 2001, pp. 235–286.
16. Karpel, M., 1990, Time Domain Aeroservoelastic Modeling Using Weighted Unsteady Aerodynamic Forces, *Journal of Guidance, Control, and Dynamics*, Vol. 13, No. 1, pp. 30–37.
17. Bendat, J. S. and Piersol, A. G., *Random Data: Analysis & Measurement Procedures, Third Edition*, John Wiley and Sons, New York, 2000.
18. Peeters, B., Lowet, G., Van der Auweraer, H., and Leuridan, J., A new procedure for modal parameter estimation, *Journal of Sound and Vibration*, 38(1), pp. 24-29, 2004.
19. Tehrani, M. G., Elliott, R.N.R., and Mottershead, J.E., 2010, Partial pole placement in structures by the method of receptances: theory and experiments, *Journal of Sound and Vibration*, 329 (24), pp. 5017-5035.
20. Ardelean, E.V. and Clark R.L., V-Stack Piezoelectric Actuator, *SPIE Smart Structures and Materials*, 4333, 2001, 322–333.
21. Ardelean, E.V., McEver, M.A., Cole D.G. and Clark R.L., Active flutter control with V-stack piezoelectric flap actuator*, AIAA Journal of Aircraft*, 43(2), 2006, 482-486.
22. Zimmerman, N.H. and Weissenburger, J.T., Prediction of flutter onset speed based on flight testing at subcritical speeds, *AIAA Journal of Aircraft*, 1(4), 190-202, 1964.
23. Price, S.J. and Lee, B.H.K., Evaluation and extenstion of the flutter-margin method for flight flutter prediction, *AIAA Journal of Aircraft,* 30(3), 395-402, 1993.
24. Dimitriadis. G. and Cooper, J.E., Flutter prediction from flight flutter test data, *AIAA Journal of Aircraft,* 38(2), 355-367, 2001.
25. Da Ronch, A., Badcock, K. J., Wang, Y., Wynn, A., and Palacios, R. N., Nonlinear Model Reduction for Flexible Aircraft Control Design, *AIAA Atmospheric Flight Mechanics Conference*, 13-16 August 2012, Minneapolis, Minnesota, AIAA 2012-4404, doi: 10.2514/6.2012-4404
26. Da Ronch, A., Tantaroudas, N. T., and Badcock, K. J., Reduction of Nonlinear Models for Control Applications, *54th AIAA/ASME/ASCE/AHS/ASC Structures, Structural Dynamics, and Materials Conference*, 8-11 April 2013, Boston, Massachusetts, AIAA 2013-1491, doi: 10.2514/6.2013-1491
27. Da Ronch, A., Tantaroudas, N. T., Timme, S., and Badcock, K. J., Model Reduction for Linear and Nonlinear Gust Loads Analysis, *54th IAA/ASME/ASCE/AHS/ASC Structures, Structural Dynamics, and Materials Conference*, 8-11 April 2013, Boston, Massachusetts, AIAA 2013-1492, doi: 10.2514/6.2013-1492